Vol. 15, No. 4, 2024
ISSN 2233-4203/ e-ISSN 2093-8950
ARTICLE www.msletters.org | Mass Spectrometry Letters

Investigation of Monomer and Oligomer Complexes of the Amyloidogenic Human Islet Amyloid Polypeptide 1-19 and Non-amyloidogenic Rat Islet Amyloid Polypeptide 1-19 by Electrospray Ionization-tandem Mass Spectrometry

Seo Yeon Kim[1] and Ho-Tae Kim[1]*

[1]*Department of Chemistry and Bioscience, Kumoh National Institute of Technology, 61, Daehak-ro, Gumi, Gyeongbuk, Republic of Korea, 39177*

Received November 29, 2024, Revised December 9, 2024, Accepted December 9, 2024
First published on the web December 31, 2024; DOI: 10.5478/MSL.2024.15.4.195

Abstract : The monomer and oligomer peptide complexes of the amyloidogenic human islet amyloid polypeptide 1-19 (hIAPP19) and non-amyloidogenic rat islet amyloid polypeptide 1-19 (rIAPP19) were investigated using electrospray ionization (ESI)-mass spectrometry (MS). The dissociation of monomers and oligomers was investigated by tandem mass spectrometry (MS/MS) using collision-induced dissociation (CID). Peptide bond dissociation in the Arg8–Ser19 region of hIAPP19 was mainly observed in the tandem mass spectra of the monomers and oligomers. The fragmentation pattern of the hIAPP19 D^{3+} (= $[dimer+3H]^{3+}$) complex was similar to that of the M^{2+} (= $[monomer+2H]^{2+}$) tandem mass spectrum in the form of {M + (fragment ion of M^{2+})}. In the case of the hIAPP T^{4+} (= $[trimer+4H]^{4+}$) complex, the $(monomer–D^{3+})^{4+}$ complex geometry was assumed to be stable based on the presence of {M + (fragment ion of D^{3+})} ions in the tandem mass spectrum of the T^{4+} complex. The interaction geometry of [(disulfide bond (S-S) in Cys2 - Cys7 region)–((S-S) in Cys2 - Cys7 region)] was proposed for the dimer and trimer complexes of hIAPP19 based on the observation of three characteristic fragment ions: (i) $[M-S]^{2+}$, $[M+S]^{2+}$, $[D-S]^{3+}$, and $[D+S]^{3+}$, (ii) y_{18}, and (iii) b_u (u = 8–18) fragment ion series in the Arg8 - Ser19 region. The tandem mass spectrum of rIAPP19 differed from that of hIAPP19. Fragment ions originating from the Cys2–Cys7 region were observed in the M^{2+} tandem mass spectrum of rIAPP19 as $[y_n+S]^{2+}$ (n = 13 – 17) and $[z_n+S]^{2+}$ (n = 13 – 15).

Keywords : hIAPP1-19, rIAPP1-19, hIAPP1-19 oligomer, rIAPP1-19 dimer, collision-induced dissociation (CID), mass spectrometry (MS), tandem mass spectrometry (MS/MS)

Introduction

The pathology of type-2 diabetes is attributed to amyloid plaques that contain fibrillar aggregates of the human islet amyloid polypeptide (hIAPP), a 37-residue hormone selectively expressed in pancreatic β-cells.[1,2] There has been considerable interest in the interaction site and process of hIAPP oligomer.[3,4] Understanding the structure and formation of early hIAPP aggregates is a prospectively important platform for the study of therapeutic agents for inhibiting disease-related structures. N-terminal helix-to-helix interactions in the 8−18 residue region[5–7] and the β-hairpin feature interactions at residues 11−18 and 23−32[8–10] have been reported using different experimental methods. The dynamics of the α-helix to β-sheet conformational transitions during the dimerization process has also been reported by simulation methods.[11,12]

Rat islet amyloid polypeptide (rIAPP), a 37-residue peptide differing from hIAPP by six residues in the 18–29 residue region, is known not to form amyloid fibrils.[13,14] Two different rIAPP D^{5+} conformations were observed based on the ion-mobility spectrometry (IMS)-MS arrival time distribution.[9] The coil-rich rIAPP dimers are formed, often with reduced amounts of helix relative to the corresponding monomers. The stable gas-phase rIAPP oligomers were also observed during CID experiments.[15] It was suggested that the α-helix region plays a crucial role in self-association with the 3D structure of rIAPP in the presence of a membrane.[13] The structures of rIAPP dimers and oligomers have been studied using molecular dynamics simulations.[16,17] It has been established that the dimer structure of rIAPP is distinct from that of hIAPP because rIAPP displays an α-helix in the N-terminal, with a distortion in the middle of the chain, followed by a second shorter α-helix,

*Reprint requests to Ho-Tae Kim
https://orcid.org/0000-0002-1541-3081
E-mail: hotaekim@kumoh.ac.kr

and is devoid of β-sheets.[16]

CID-MS/MS experiments are performed to obtain structural information of the non-covalent complexes, which are conducted by mass-extracting a specific dimer or oligomeric complex and then measuring its collision induced fragment ions to infer the non-covalent complex geometry. In case of hIAPP dimer, the peptide bond dissociation fragment ions in the 15–37 residue region of the monomer subunit were observed under low-collision energy conditions.[18]

The proposed hIAPP dimer structure, which has [(N-terminal)–(N-terminal)] interaction geometry, is likely different from those observed in the IMS-MS experiments and subsequent MD simulations of the +6 dimer structures.[9] The importance of the N-terminal helical interaction of hIAPP has been also studied[19,20] by hIAPP19, which form a helical interaction complex when bound to the membrane. rIAPP19 is considerably less toxic than hIAPP19 even though it differs from hIAPP19 by only one residue (substitution of arginine for histidine at residue 18). Fisher et al.[21] proposed the importance of the disulfide bonds between Cys2 and Cys7 in the "native" amylin oligomers. Removal of the disulfide bonds in the "native" amylin oligomers decreases the original polymorphism structure and induces the formation of stable cross-β strands in the N-termini. Camargo et al.[22] proposed that the redox environment triggers conformational changes and aggregation of hIAPP in the N-terminal disulfide bond regions.

In this study, we used CID in conjunction with ESI-MS to obtain structural information on hIAPP19 monomer, dimer, and trimer complexes for comparison with the structures of rIAPP19 monomeric and dimeric complexes. hIAPP19 (or rIAPP19) oligomeric complexes were allowed to form in the solution and electrosprayed onto a quadrupole ion guide. The fragmentation patterns of the hIAPP19 (or rIAPP19) oligomers were investigated in a 50 % H_2O+50% CH_3OH solution. In previous studies, we investigated multiply charged monomers and dimers of hIAPP and rIAPP using low-energy CID tandem mass spectrometry.[18, 23]

Experimental

A Thermo Finnigan LTQ mass spectrometer (Thermo Fisher Scientific, Waltham, MA, USA) was used to obtain MS and MS/MS spectra for the hIAPP19 (or rIAPP19) oligomeric fragmentation pattern analysis. The LTQ is a linear ion trap mass spectrometer equipped with an atmospheric pressure ESI source.

MS Conditions

hIAPP19 (or rIAPP19) oligomeric complex samples were introduced into the electrospray interface via direct infusion using a microsyringe pump at a flow rate in the range of 1–2 mL min^{-1}. The heated capillary temperature was set at 200°C to facilitate efficient complex formation. Positive-ion MS spectra were acquired over an *m/z* range of 100–2000 by averaging 1000–6000 scans. The MS/MS experimental conditions were as follows: ion-trap pressure, 1×10^{-5} Torr; activation time, 30 ms; injection time, 100–200 ms, and isolation width, 0.6–1.5 mass units. The parent hIAPP19 (or rIAPP19) oligomeric complex ions were individually and manually selected and subjected to CID. The collision energy of CID process was optimized for each MS/MS experiment to obtain sufficiently high signal-to-noise ratios.

Reagents

hIAPP19 synthetic peptide (purity > 95%, amidated at the C-terminus KCNTATCATQRLANFLVHS-NH_2, Peptron, Daejeon, Korea), rIAPP19 synthetic peptide (purity > 95%, amidated at the C-terminus KCNTATCATQRLANFLVRS- NH_2, Peptron, Daejeon, Korea), H_2O (HPLC grade, Merck Ltd., Korea), and CH_3OH (HPLC grade; Merck Ltd., Korea) were used in the experiments. The hIAPP19 peptide solutions were prepared in a 50% H_2O+50% CH_3OH solution at a final concentration of 60 μM and rIAPP19 for 100 μM. These solutions were prepared to obtain sufficient amounts of D^{3+} intensity for the CID-MS/MS experiments. The experiments were performed within 24 h following sample preparation.

Results and Discussion

MS Spectra

Under the ESI experimental conditions, the mass spectra of hIAPP19 and rIAPP19 solutions included multiple charged monomers and oligomers (Figure 1). hIAPP19 monomers were observed at *m/z* 1038.0, 692.3, and 519.5 (ranging from 2+ to 4+), and from M^{2+} to M^{4+} in multiple proton-adduct forms. The hIAPP19 peptide contains three basic residues (Lys1, Arg11, and His18) and an N-terminal residue available for protonation. The M^{5+} peak at *m/z* 415.8 was not observed in the ESI-MS spectrum of the hIAPP19 solution (Figure 1). The M^{3+} monomer was observed as a high-intensity peak. For the oligomers, peaks were observed with noticeable intensities at *m/z* 1383.7 and 1556.5, corresponding to D^{3+} and T^{4+}, respectively. In the case of rIAPP19, monomers were observed at *m/z* 1047.5, 698.7, and 524.3 (ranging from 2+ to 4+) with multiple proton adducts. The *m/z* 1396.4 peak for D^{3+} was also observed with very low intensity (Figure 1b). This may be explained by the propensity for nonamyloidogenic characteristics.

MS/MS Spectra of hIAPP19 (or rIAPP19) Monomer

CID-MS/MS experiments were performed to obtain the fragmentation pattern spectra for M^{2+}–M^{4+} of the hIAPP19 peptide, as shown in Figure 2. The fragment ions were labeled with various colors and shapes based on the fragment residue regions to compare the fragmentation

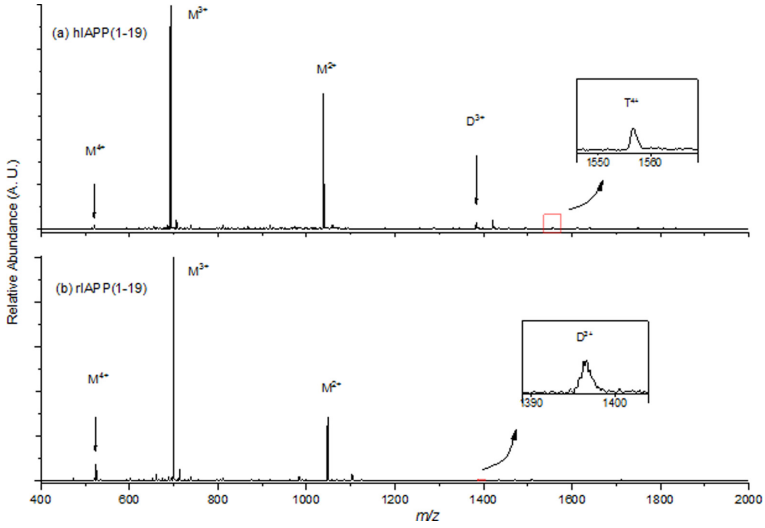

Figure 1. ESI-MS spectrum of hIAPP19 and rIAPP19 solution. Multiply charged monomers and oligomers are represented as M^{z+} (z = 2, 3, and 4 charge states, M = hIAPP19 or rIAPP19 monomer), D^{3+}, and T^{4+} (D = dimer and T = Trimer).

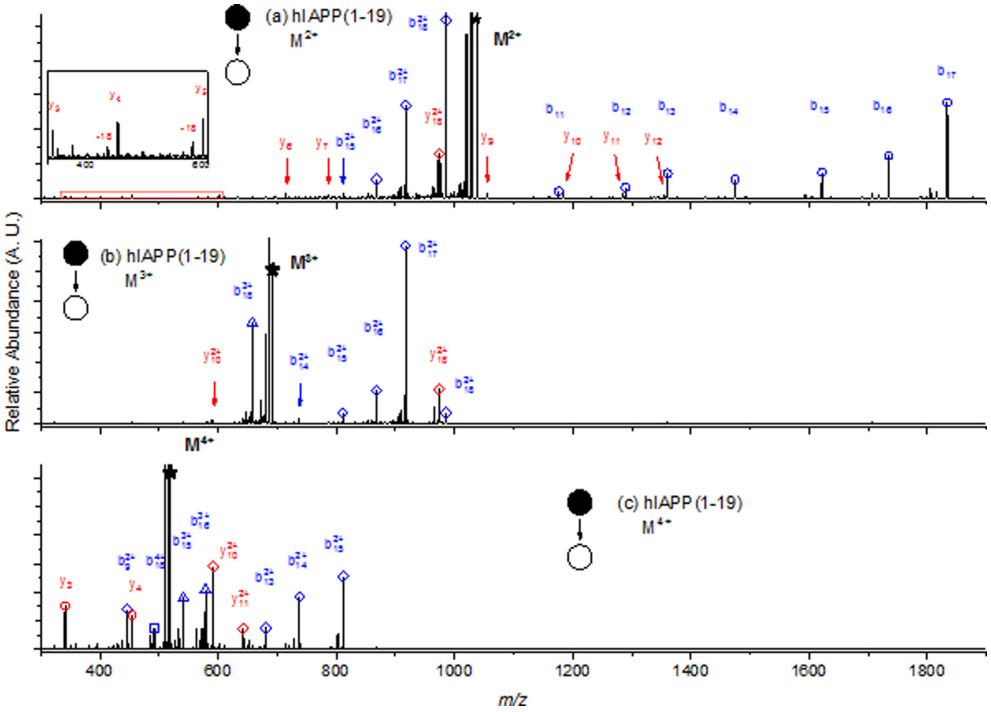

Figure 2. MS/MS spectra of (a) M^{2+}, (b) M^{3+}, and M^{4+} hIAPP19 parent ion. The charge states are distinguished by different shapes (1+ = circle, 2+ = diamond, 3+ = triangle, 4+ = square). The b-, and y-fragment ions are indicated by blue and red colors, respectively. For simplicity, the (1+) charge state is omitted in the fragment "b" and "y" ion series, $b_{15} = b_{15}^{1+}$ and $y_{12} = y_{12}^{1+}$.

patterns of each parent ion. The b- and y-fragment ions were observed in the Lys1-Cys2 and Arg8-Ser19 regions (Figure 2). In the case of the M^{2+} tandem mass spectrum of the hIAPP19, y_{18}^{2+} and ① b_{11}–b_{17} (or counter fragment ion y_3–y_{12}) ions are observed in Figure 2a and are shown as characteristic fragment ions in Table 1 and Scheme 1a. MS/MS fragmentation pattern of hIAPP19 M^{2+} will be useful for analyzing hIAPP19 oligomer MS/MS spectra. Interestingly, the peptide bond dissociation channels between Cys2 and Cys7 were not observed in the hIAPP19 monomer tandem mass spectra, regardless of the monomeric ion charge state. It is conjectured that the disulfide bond between the Cys2 and Cys7 side groups does not dissociate to low-energy CID processes. The fragment ions are listed in Table

Table 1. Comparison of MS/MS fragment ions of hIAPP19 (or rIAPP19) monomer and oligomers. Fragment "b" and "y" ions were observed in the MS/MS spectrum of hIAPP19 (or rIAPP19) monomer. (M + b) and (M + y) fragment ions were observed in the MS/MS spectrum of the hIAPP19 (or rIAPP19) dimer complex. The S-S disulfide bond dissociation fragments ions are also observed in the MS/MS spectra of hIAPP19 (or rIAPP19) monomer and oligomers.

Parent ion		MS/MS fragment ions			
		Lys1	Cys2-Cys7 1region	Arg8-Ser19 region	Characteristic ions
hIAPP19	M^{2+}	y_{18}^{2+}	N/A	b_u (u = 11 – 17) y_n (n = 3 – 12), b_u^{2+} (u = 15 – 18)	① b_u (u = 11 – 17)
	M^{3+}	y_{18}^{2+}	N/A	y_{10}^{2+}, b_u^{2+} (u = 14 – 18), b_{18}^{3+}	
	D^{3+}	$[M + y_{18}]^{3+}$	$[M - S]^{2+}$, $[M + S]^{2+}$	$[M + b_u]^{2+}$ (u = 8 – 17)	② $[M + ①]^{2+}$ ③ $[M - S]^{2+}$, $[M + S]^{2+}$
	T^{4+}	$[2M+y_{18}]^{4+}$	$[M - S]^{2+}$, $[M + S]^{2+}$ $[D - S]^{3+}$, $[D + S]^{3+}$	$[2M + b_u]^{3+}$ (u = 13 – 17)	④ $[2M + ①]^{3+}$ ⑤ $[M + ③]^{3+}$, ③
rIAPP19	M^{2+}	y_{18}^{2+}, z_{18}	y_{13} - S, z_{13} - S $(z_n + S)^{1+}$ (n = 13 – 15) $(y_n + S)^{2+}$ (n = 13– 17)	b_u (u = 11 – 17) y_n (n = 3 – 12) b_u^{2+} (u = 15 – 18) y_{12}^{2+}	① b_u (u = 11 – 17) ⑥ $(z_n + S)^{1+}$ (n = 13 – 15) $(y_n + S)^{2+}$ (n = 13 – 17) y_{13} – S, z_{13} – S ⑦ y_{12}^{2+}
	M^{3+}	y_{18}^{2+}	$(y_n + S)^{2+}$ (n = 13 – 17)	y_n (n = 3 – 6), y_n^{2+} (n = 9 – 11) b_u^{2+} (u = 15 – 18)	
	D^{3+}	$[M + y_{18}]^{3+}$	z_{13} - S, $[M - S]^{2+}$ $[M + S]^{2+}$	y_{12}^{2+}, x_{12}^{2+}	③ , ⑥ z_{13}-S ⑦ y_{12}^{2+}

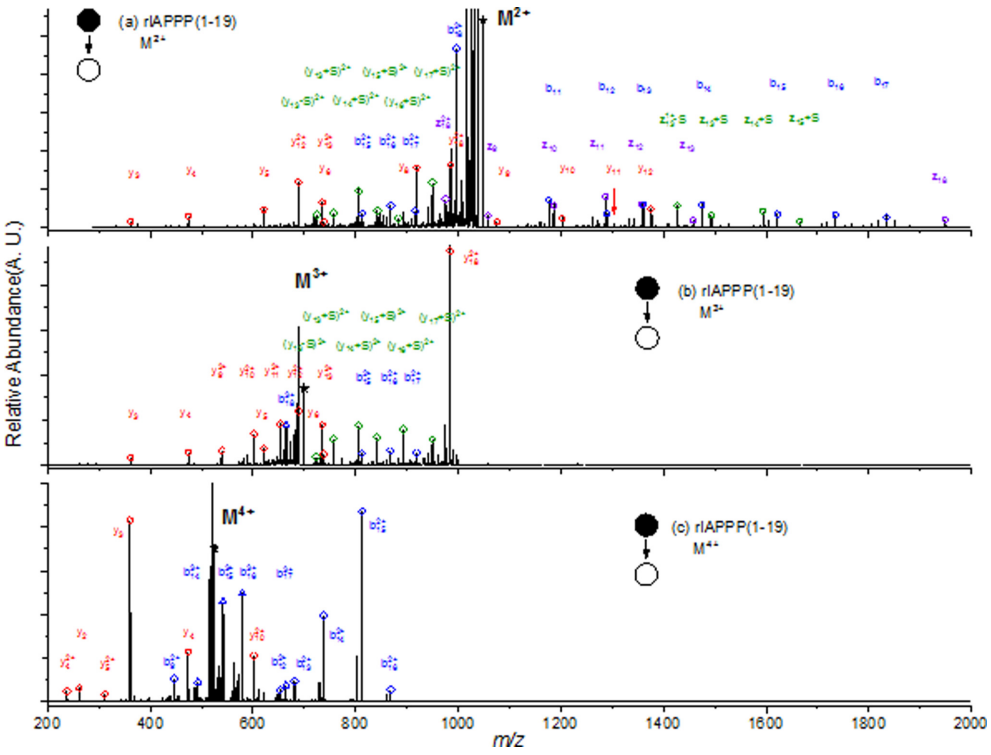

Figure 3. MS/MS spectra of (a) M^{2+}, (b) M^{3+}, and M^{4+} rIAPP19 parent ion. The charge states are distinguished by different shapes (1+ = circle, 2+ = diamond, 3+ = triangle, 4+ = square). The S-S disulfide bond dissociation, b-, and y-fragment ions are indicated by green, blue, and red colors, respectively. For simplicity, the (1+) charge state is omitted in the fragment "b" and "y" ionic series, $b_{15} = b_{15}^{1+}$ and $y_{12} = y_{12}^{1+}$.

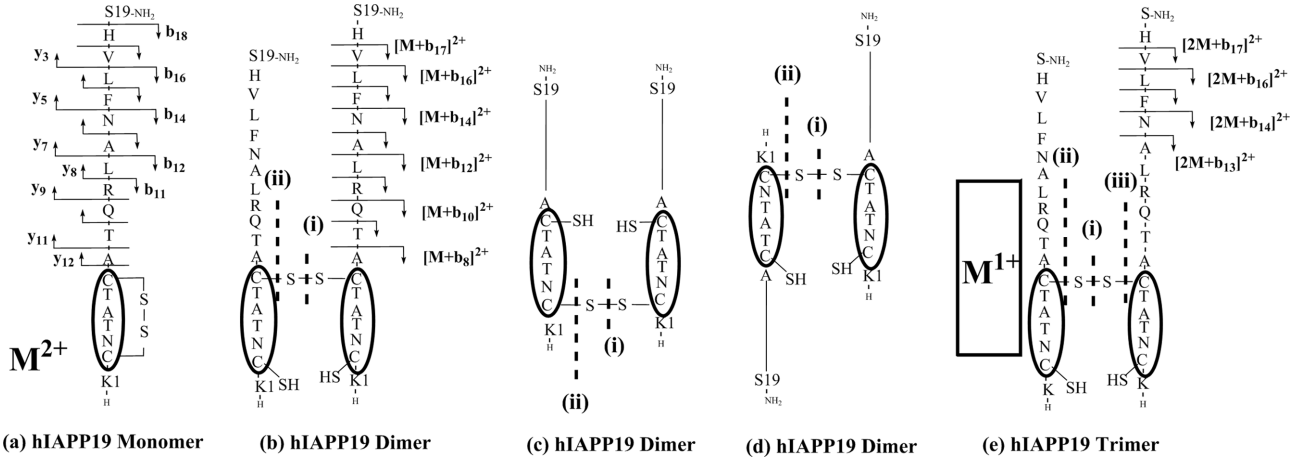

Scheme 1. (a) hIAPP19 monomer sequence along with fragmentation M^{2+} sites and schematics of proposed hIAPP19 dimer and trimer complex. Schematics of structures (b)-(d) of proposed hIAPP19 dimer. The observed $[M + b_u]^{2+}$ (u = 8 – 17) fragment ions are indicated in (b). (e) Schematics of proposed hIAPP19 trimer.

1. The *m/z* values and assignments of the fragment ions are presented in Electronic Supplementary Information (Table S1-S2). The M^{2+} tandem mass spectra of rIAPP19 were completely different from those of hIAPP19 during the dissociation of the Cys2-Cys7 region. The y- and z-fragment[24,25] ions, $(z_{13} + S)^{1+} - (z_{15} + S)^{1+}$ and $(y_{13} + S)^{2+} - (y_{17} + S)^{2+}$, were observed during the disulfide bond cleavage process. The basic part of the R18 side group in rIAPP19 is supposed to attack part of the disulfide bond, similar to the disulfide bond reduction process described previously.[26, 27] The schematic diagram of rIAPP19 M^{2+} monomer is presented in Electronic Supplementary Information (Scheme S1). The b- and y-fragment ions of rIAPP19 M^{2+} tandem mass spectra were similar to those of hIAPP19 as the observed fragmentation patterns in the Lys1-Cys2 and Arg8-Ser19 regions (Figure 3a), except for the considerably high-intensity y_{12}^{2+} fragment ion. The y_{12}^{2+} fragment ion was not detected in the MS/MS spectrum of the hIAPP19 M^{2+} parent ion (Figure 2a). It is worth noting that the $(y_{13} + S)^{2+} - (y_{17} + S)^{2+}$ fragmentation pattern is not observed in the M^{4+} tandem mass spectrum (Figure 3c). The S-S disulfide bond geometry of the M^{4+} complex is assumed to differ from that of the M^{2+} or M^{3+} complexes due to the addition of protons depending on the charge state.

MS/MS Spectra of hIAPP19 (or rIAPP19) Oligomer

Two dissociation channels were observed in the MS/MS spectrum of the hIAPP19 dimer (Figure 4a). The peptide bond dissociation in the Arg8-Ser19 region (② $[M + b_u]^{2+}$ (u = 8 – 17)) and the disulfide bond dissociation in the Cys2-Cys7 region (③$[M - S]^{2+}$ and $[M + S]^{2+}$) which is not observed in the MS/MS spectrum of hIAPP19 monomers. The fragmentation pattern of the peptide bond dissociation in the Arg8-Ser19 region (②$[M + b_u]^{2+}$ (u = 8 – 17)) is the form of $\{(M^{1+}) + ②\}$ ions, which is the same as those shown in the M^{2+} tandem mass spectrum (Figure 2a), except for the M^{1+} component in the form of $\{(M^{1+}) + ②\}$ions. Therefore, the observed CID-MS/MS fragmentation pattern shown in Figure 4a was expected to originate from the M^{2+} monomer component of the $\{M^{1+} + M^{2+}\}$ dimer geometry. The entire M^{1+} component is thought to be conserved throughout the MS/MS dissociation of the D^{3+} complex. The possible structure of the hIAPP19 D^{3+} complex is shown in Scheme 1b. The hIAPP19 dimer geometry in Scheme 1b is similar to the {(S-S disulfide bond) – (S-S disulfide bond)} interaction geometry in the previously reported disulfide bond cleavage process.[26,27]

During the disulfide bond dissociation in the Cys2-Cys7 region, the D^{3+} complex was separated into three possible components: ③$[M - S]^{2+}$, $[M + S]^{2+}$, and M^{2+}, as shown in Figure 4a. The M^{1+} *m/z* value of 2075.0 is beyond the *m/z* range of our MS/MS spectrum. The two proposed (S-S) disulfide bond dissociation channels (i) and (ii) are shown in Scheme 1b-d. The proposed D^{3+} structures (Scheme 1b-d) were based on the observation of the $[M – S]^{2+}$ and $[M + S]^{2+}$ fragment ions. The Scheme 1b-c geometries are shown as the parallel-geometry structures and an antiparallel geometry structure is shown in Scheme 1d. The T^{4+} fragmentation pattern in the peptide bond dissociation of Arg8-Ser19 region, ④ $[2M + b_u]^{3+}$ (u = 13 – 17), is the form of $\{(2M^{1+}) + ②\}$ ions which is exactly the same as those shown in the M^{2+} tandem mass spectrum (Figure 2a) except for the $(2M^{1+})$ component in the form of $\{(2M^{1+}) + ②\}$ ions. The fragmentation pattern of $[M + \{M + b_u\}]^{3+}$ (u = 13 – 17) was analyzed using the fragmentation form of {M+ (fragment ions of D^{3+})}. Therefore, the observed CID-MS/MS fragmentation pattern shown in Figure 4b was expected to originate from the D^{3+} dimer component of the $[\text{monomer–(Di+3H)}^{3+}]^{4+}$ complex. The possible geometry of the hIAPP19 T^{4+} structure, including the {(S-S disulfide

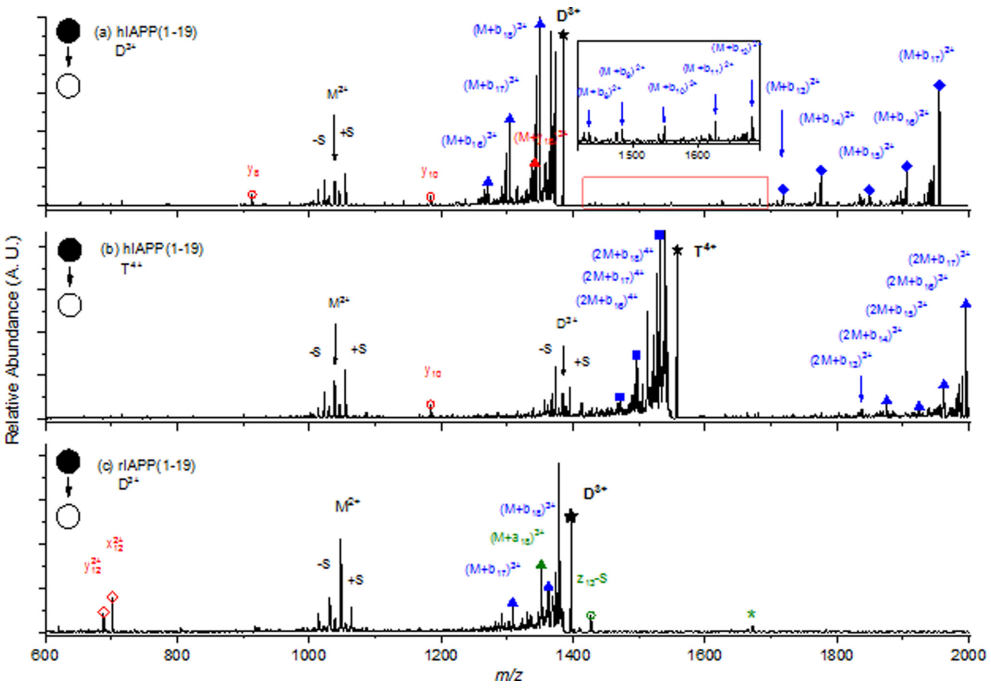

Figure 4. MS/MS spectra of (a) hIAPP19 D^{3+}, (b) hIAPP19 T^{4+}, and (c) rIAPP19 D^{3+} ions. The charge states are distinguished by different shapes (1+ = circle, 2+ = diamond, 3+ = triangle, 4+ = square). The a-, b-, and y- fragment ions are indicated by green, blue, and red colors, respectively. The empty and filled shapes indicate the existence of monomer ions in the fragment ions. The asterisk ions are the fragment ions resulting from the (1+) ions stored at the same time as the rIAPP D^{3+} ions in the LTQ ion trap.

bond)–(S-S disulfide bond)} interaction geometry of the D^{3+} dimer complex, is illustrated in Scheme 1e. The three monomers of the T^{4+} structure were supposed to be aligned in the geometric order of $\{M^{1+} + M^{1+} + M^{2+}\}$ instead of $\{M^{1+} + M^{2+} + M^{1+}\}$ because the $\{M^{1+} + M^{2+} + M^{1+}\}$ geometry is difficult to explain the observation of two fragment ions in Figure 4b, $\{(2M^{1+}) + ②\}$ ionic series and the M^{2+} fragment ion.

The disulfide bond dissociation in the Cys2-Cys7 region was also observed as the form of ⑤ $[D – S]^{3+}$ and $[D + S]^{3+}$ in the MS/MS spectrum of the hIAPP19 trimer complex (Figure 4b). These ⑤ $[D – S]^{3+}$ and $[D + S]^{3+}$ fragment ions mimic the form of dimer $[M – S]^{2+}$ and $[M + S]^{2+}$ fragment ions like the form of $\{M^{1+} + ③\}$. The possible dissociation channels, (ii) $[D - S]^{3+}$ and (iii) $[D + S]^{3+}$, are proposed in Scheme 1e. The disulfide bond dissociation in the Cys2-Cys7 region, ③ $[M – S]^{2+}$ and $[M + S]^{2+}$ and two M^{2+} characteristic fragment ions (⑥ z_{13}-S and ⑦ y_{12}^{2+}), were observed in the MS/MS spectrum of rIAPP19 dimer complex. It is expected that the rIAPP19 dimer has a {monomer–M^{2+}} geometric structure. However, as ① b_u (u = 11 – 17) and ⑥ $\{(z_n + S)^{1+}$ (n = 13–15), $(y_n + S)^{2+}$ (n = 13 – 17)} characteristic fragmentation patterns are not observed in Figure 4c, it is considered that the original rIAPP19 M^{2+} geometry is not maintained in the form of the {monomer–M^{2+}} rIAPP19 dimer complex geometry.

Conclusion

CID-MS/MS experiments were conducted to obtain structural information on the hIAPP19 monomer, dimer, and trimer complexes for comparison with the structures of the rIAPP19 monomeric and dimeric complexes. Schematic hIAPP19 dimer and trimer structures (Schemes 1b-e) are proposed based on the {M + ①, ②, or ③} fragment ions, which have the form of {M + fragment ions of M^{2+} or D^{3+}}. The schematic geometries of the D^{3+} complex, the interaction geometry of {(S-S disulfide bond)–(S-S disulfide bond)}, are proposed in Scheme 1b-d based on the observation of ③$[M - S]^{2+}$ and $[M + S]^{2+}$ fragment ions in the tandem mass spectrum of the hIAPP19 D^{3+} complex. The T^{4+} complex geometry is proposed to be aligned in the geometric order of $\{M^{1+} + M^{1+} + M^{2+}\}$ based on the observation of the form of $\{(2M^{1+}) + ②\}$ ionic series and M^{2+} fragment ions in the tandem mass spectrum of the hIAPP19 T^{4+} complex.

Acknowledgments

This research was supported by Basic Science Research Program through the National Research Foundation of Korea (NRF) funded by the Ministry of Education (RS-2021-NR066247).

Notes

Electronic Supplementary Information (ESI) is available [details of any available supplementary information should be included here]. See DOI: xxxx/xxxxx. /

References

1. Guo, J.; Sun, W.; Li, L.; Liu, F.; Lu, W.; *RSC Advances*, **2017**, 7, 43491. https://doi.org/10.1039/c7ra05742c
2. Cooper, G. J. S.; Willis, A. C.; Clark, A.; Turner, R. C.; Sim, R. B.; Reid, K. B. M.; *Proc. Natl. Acad. Sci. USA*, **1987**, 84, 8628. https://doi.org/10.1073/pnas.84.23.8628
3. Liang, G.; Zhao, J.; Yu, X.; Zheng, J.; *Biochemistry*, **2013**, 52, 1089. https://doi.org/10.1021/bi301525e
4. Chiu, C.-C.; de Pablo, J. J.; *AIP Advances*, **2015**, 5, 092501. https://doi.org/10.1063/1.4921073
5. Wiltzius, J. J. W.; Sievers, S. A.; Sawaya, M. R.; Eisenberg, D.; *Protein Science*, **2009**, 18, 1521. https://doi.org/10.1002/pro.145
6. Zhao, D.-S.; Chen, Y.-X.; Li, Y.-M.; *Chem. Commun.*, **2015**, 51, 2095. https://doi.org/10.1039/c4cc06739h
7. Nagel-Steger, L.; Owen, M. C.; Strodel, B.; *ChemBioChem*, **2016**, 17, 657. https://doi.org/10.1002/cbic.201500623
8. Dupuis, N. F.; Wu, C.; Shea, J.-E.; Bowers, M. T.; *J. Am. Chem. Soc.*, **2009**, 131, 18283. https://doi.org/10.1021/ja903814q
9. Dupuis, N. F.; Wu, C.; Shea, J.-E.; Bowers, M. T.; *J. Am. Chem. Soc*., **2011**, 133, 7240. https://doi.org/10.1021/ja1081537
10. Buchanan, L. E.; Dunkelberger, E. B.; Tran, H. Q.; Cheng, P.-N.; Chiu, C.-C.; Cao, P.; Raleigh, D. P.; de Pablo, J. J.; Nowick, J. S.; Zanni, M. T.; *Proc. Natl. Acad. Sci. USA*, **2013**, 110, 19285. https://doi.org/10.1073/pnas.1314481110
11. Qi, R.; Luo, Y.; Ma, B.; Nussinov, R.; Wei, G.; *Biomacromolecules*, **2014**, 15, 122. https://doi.org/10.1021/bm401406e
12. Qiao, Q.; Qi, R.; Wei, G.; Huang, X.; *Phys. Chem. Chem. Phys*, **2016**, 18, 29892. https://doi.org/10.1039/c6cp05590g
13. Nanga, R. P. R.; Brender, J. R.; Xu, J.; Hartman, K.; Subramanian, V.; Ramamoorthy, A.; *J. Am. Chem. Soc.*, **2009**, 131, 8252. https://doi.org/10.1021/ja9010095
14. Green, J.; Goldsbury C.; Mini, T.; Sunderji, S.; *J. Mol. Biol.*, **2003**, 326, 1147. doi:10.1016/S0022-2836(02)01377-3
15. Young, L. M.; Cao, P.; Raleigh, D. P.; Ashcroft, A. E.;Radford, S. E. *J. Am. Chem. Soc.* 2014, 136, 660. DOI:10.1021/ja406831n.
16. Laghaei, R.; Mousseau, N.; Wei, G.; *J. Phys. Chem. B,* **2011**, 115, 3146. https://doi.org/10.1021/jp108870q
17. Liang, G.; Zhao, J.; Yu, X.; Zheng, J.; *Biochemistry* **2013**, 52, 1089. https://doi.org/10.1021/bi301525e
18. Seo, J.-H.; Cha, E.; Kim, H.-T.; *Chemical Physics Letters* **2018**, 708, 61. https://doi.org/10.1016/j.cplett.2018.08.001
19. Nanga, R. P. R.; Brender, J. R.; Xu, J.; Veglia, G.; Ramamoorthy, A.; *Biochemistry* **2008**, 47, 12689. https://doi.org/10.1021/bi8014357
20. Brender, J. R.; Lee, E. L.; Cavitt, M. A.; Gafni, A.; Steel, D. G.; Ramamoorthy, A.; *J. Am. Chem. Soc.*, **2008**, 130, 6424. https://doi.org/10.1021/ja710484d
21. Wineman-Fisher, V.; Tudorachi, L.; Nissim, E.; Miller, Y.; *Phys. Chem. Chem. Phys*., **2016**, 18, 12438. https://doi.org/10.1039/c6cp01196a
22. Rodriguez Camargo, D. C.; Tripsianes, K.; Buday, K.; Franko, A.; Göbl, C.; Hartlmüller, C.; Sarkar, R.; Aichler, M.; Mettenleiter, G.; Schulz, M.; Böddrich, A.; Erck, C.; Martens, H.; Walch, A. K.; Madl, T.; Wanker, E. E.; Conrad, M.; Hrabě de Angelis, M.; Reif, B.; *Scientific Reports*, **2017**, 7:44041. https://doi.org/10.1038/srep44041
23. Kim, J.; Kim, H.-T.; *Mass Spectrom. Lett.,* **2021**, 12, 179. https://doi.org/10.5478/MSL.2021.12.4.179
24. Chung, T. W.; Hui, R.; Ledvina, A.; Coon, J. J.; Tureček, F.; *J. Am. Soc. Mass Spectrom*., **2012**, 23, 1336. https://doi.org/10.1007/s13361-012-0408-9
25. Han, H.; Xia, X.; and McLuckey, S. A.; *Journal of Proteome Research,* **2007**, 6, 3062. https://doi.org/10.1021/pr070177t
26. Fujimoto, T,; Inaba, K.; and Kadokura, H.; *Protein Science*, **2019**, 28, 30. https://doi.org/10.1002/pro.3530
27. Cook, K. M.; and Hogg, P. J.; *Antioxidants & Redox Signaling,* **2013**, 18, 1987. https://doi.org/10.1089/ars.2012.4807